Improved bounds on the dipole moments of the tau neutrino from high-energy $\gamma^* e^-$ and $\gamma^*\gamma^*$ collisions at the ILC and CLIC

A. Gutiérrez-Rodríguez,[1,*] M. Koksal,[2,†] and A. A. Billur[2,‡]

[1]*Facultad de Física, Universidad Autónoma de Zacatecas, Apartado Postal C-580, 98060 Zacatecas, México*

[2]*Deparment of Physics, Cumhuriyet University, 58140 Sivas, Turkey*

(Received 5 December 2014; published 22 May 2015)

In this work we study the potential of the processes $e^+e^- \to e^+\gamma^* e^- \to e^+\tau\bar{\nu}_\tau\nu_e$ and $e^+e^- \to e^+\gamma^*\gamma^* e^- \to e^+\nu_\tau\bar{\nu}_\tau e^-$ at a future high-energy and high-luminosity linear electron positron collider, such as the International Linear Collider and Compact Linear Collider, to study the sensibility on the anomalous magnetic and electric dipole moments of the tau neutrino. For an integrated luminosity of 590 fb^{-1} and center-of-mass energy of 3 TeV, we derive 95% C.L. limits on the dipole moments: $\mu_{\nu_\tau} \leq 1.44 \times 10^{-6}\mu_B$ and $d_{\nu_\tau} \leq 2.78 \times 10^{-17} ecm$ in the $\gamma^* e^-$ collision mode and of $\mu_{\nu_\tau} \leq 3.4 \times 10^{-7}\mu_B$ and $d_{\nu_\tau} \leq 6.56 \times 10^{-18} ecm$ with the $\gamma^*\gamma^*$ collision mode, improving the existing limits.

DOI: 10.1103/PhysRevD.91.093008 PACS numbers: 13.40.Em

I. INTRODUCTION

In the standard model (SM) [1–3] extended to contain right-hand neutrinos, the neutrino magnetic moment induced by radiative corrections is unobservably small, $\mu_\nu = 3eG_F m_{\nu_i}/(8\sqrt{2}\pi^2) \simeq 3.1 \times 10^{-19}(m_{\nu_i}/1\,\text{eV})\mu_B$, where $\mu_B = e/2m_e$ is the Bohr magneton [4,5]. Current limits on these magnetic moments are several orders of magnitude larger, so that a magnetic moment close to these limits would indicate a window for probing effects induced by new physics beyond the SM [6]. Similarly, a neutrino electric dipole moment will also point to new physics and will be of relevance in astrophysics and cosmology, as well as terrestrial neutrino experiments [7]. In the case of the magnetic moment of the ν_e the best bound is derived from globular cluster red giants energy loss [8];

$$\mu_{\nu_e} < 3 \times 10^{-12}\mu_B \tag{1}$$

is far from the SM value. The best current laboratory constraint

$$\mu_{\nu_e} < 2.9 \times 10^{-11}\mu_B, \qquad 90\%\ \text{C.L.} \tag{2}$$

is obtained in $\bar{\nu}_e - e^-$ elastic scattering experiment GEMMA [9], which is an order of magnitude larger than the constraint obtained in astrophysics [8].

For the magnetic moment of the muon neutrino the current best limit has been obtained in the LSND experiment [10]

$$\mu_{\nu_\mu} \leq 6.8 \times 10^{-10}\mu_B, \qquad 90\%\ \text{C.L.} \tag{3}$$

In the case of the electric dipole moment d_{ν_e,ν_μ} [11] the best limits are

$$d_{\nu_e,\nu_\mu} < 2 \times 10^{-21}(ecm), \qquad 95\%\ \text{C.L.} \tag{4}$$

The most general expression consistent with Lorentz and electromagnetic gauge invariance for the tau neutrino electromagnetic vertex may be parametrized in terms of four form factors:

$$\Gamma^\alpha = eF_1(q^2)\gamma^\alpha + \frac{ie}{2m_{\nu_\tau}}F_2(q^2)\sigma^{\alpha\mu}q_\mu + eF_3(q^2)\gamma_5\sigma^{\alpha\mu}q_\mu + eF_4(q^2)\gamma_5(\gamma^\mu q^2 - \not{q}q^\mu), \tag{5}$$

where e is the charge of the electron, m_{ν_τ} is the mass of the tau neutrino, q^μ is the photon momentum, and $F_{1,2,3,4}(q^2)$ are the electromagnetic form factors of the neutrino, corresponding to charge radius, magnetic moment, electric dipole moment, and anapole moment, respectively, at $q^2 = 0$ [12–18]. The form factors corresponding to charge radius and the anapole moment do not concern us here.

The current best limit on μ_{ν_τ} has been obtained in the Borexino experiment, which explores solar neutrinos. Searches for the magnetic moment of the tau neutrino have also been performed in accelerator experiments. The experiment E872 (DONUT) is based at $\nu_\tau e^-, \bar{\nu}_\tau e^-$ elastic scattering. In the CERN experiment WA-066, a limit on μ_{ν_τ} is obtained on an assumed flux of tau neutrinos in the neutrino beam. The L3 collaboration obtain a limit on the magnetic moment of the tau neutrino from a sample of e^+e^- annihilation events at the Z resonance. Experimental

*alexgu@fisica.uaz.edu.mx
†mkoksal@cumhuriyet.edu.tr
‡abillur@cumhuriyet.edu.tr

TABLE I. Experimental limits on the magnetic moment of the tau neutrino.

Experiment	Method	Limit	C. L.	Reference
Borexino	Solar neutrino	$\mu_{\nu_\tau} < 1.9 \times 10^{-10}\mu_B$	90%	[19]
E872 (DONUT)	Accelerator $\nu_\tau e^-, \bar{\nu}_\tau e^-$	$\mu_{\nu_\tau} < 3.9 \times 10^{-7}\mu_B$	90%	[20]
CERN-WA-066	Accelerator	$\mu_{\nu_\tau} < 5.4 \times 10^{-7}\mu_B$	90%	[21]
L3	Accelerator	$\mu_{\nu_\tau} < 3.3 \times 10^{-6}\mu_B$	90%	[22]

limits on the magnetic moment of the tau neutrino are shown in Table I.

Other limits on the magnetic moment of the μ_{ν_τ} are reported in the literature [12,23–42].

In this work we study the sensibility of the anomalous magnetic and electric dipole moments of the tau neutrino through the processes $e^+e^- \to e^+\gamma^*e^- \to e^+\tau\bar{\nu}_\tau\nu_e$ and $e^+e^- \to e^+\gamma^*\gamma^*e^- \to e^+\nu_\tau\bar{\nu}_\tau e^-$ at a future high-energy and high-luminosity linear electron positron collider, with a center-of-mass energy in the range of 500 to 1600 GeV, such as the International Linear Collider (ILC) [43], and of 3 TeV at the Compact Linear Collider (CLIC) [44]. Not only can the future e^+e^- linear collider be designed to operate in e^+e^- collision mode, but it can also be operated as a $e\gamma$ and $\gamma\gamma$ collider. This is achieved by using Compton backscattered photons in the scattering of intense laser photons on the initial e^+e^- beams. The other well-known applications of linear colliders are to study new physics beyond the SM through $e\gamma^*$ and $\gamma^*\gamma^*$ collisions. A quasireal γ^* photon emitted from one of the incoming e^- or e^+ beams can interact with the other lepton shortly after, and the subprocess $\gamma^*e^- \to \tau\bar{\nu}_\tau\nu_e$ can generate. Hence, first, we calculate the main reaction $e^+e^- \to e^+\gamma^*e^- \to e^+\tau\bar{\nu}_\tau\nu_e$ by integrating the cross section for the subprocess $\gamma^*e^- \to \tau\bar{\nu}_\tau\nu_e$. Also, γ^* photons emitted from both e^- and e^+ beams collide with each other, and the subprocess $\gamma^*\gamma^* \to \nu_\tau\bar{\nu}_\tau$ can be produced. Second, we find the main reaction $e^+e^- \to e^+\gamma^*\gamma^*e^- \to e^+\nu_\tau\bar{\nu}_\tau e^-$ by integrating the cross section for the subprocess $\gamma^*\gamma^* \to \nu_\tau\bar{\nu}_\tau$. In both cases, the quasireal photons in $e\gamma^*$ and $\gamma^*\gamma^*$ collisions can be examined by equivalent photon approximation (EPA) [45–47], which is to say, by using the Weizsacker-Williams approximation. In EPA, photons emitted from incoming leptons which have very low virtuality are scattered at very small angles from the beam pipe and because the emitted quasireal photons have a low Q^2 virtuality these are almost real. These processes have been observed experimentally at the LEP, Tevatron, and LHC [48–54]. In particular, the most stringent experimental limit on the anomalous magnetic dipole moment of the tau lepton is obtained through the process $e^+e^- \to e^+\gamma^*\gamma^*e^- \to e^+\tau\bar{\tau}e^-$ by using multiperipheral collision at the LEP [55].

In Refs. [56,57], the electromagnetic properties of the neutrinos were examined via the Weizsacker-Williams approximation at the LHC. In Ref. [56] nonstandard couplings $\nu\bar{\nu}\gamma$ and $\nu\bar{\nu}\gamma\gamma$ were investigated via $\nu\bar{\nu}q$ production in the process $pp \to p\gamma^*p \to p\nu\bar{\nu}qX$. In addition, the potential of $\gamma^*\gamma^*$ collisions at the LHC was studied via the reaction $pp \to p\gamma^*\gamma^*p \to p\nu\bar{\nu}p$ to probe neutrino-photon coupling by Ref. [57].

With these motivations, we study the potential of the processes $e^+e^- \to e^+\gamma^*e^- \to e^+\tau\bar{\nu}_\tau\nu_e$ and $e^+e^- \to e^+\gamma^*\gamma^*e^- \to e^+\nu_\tau\bar{\nu}_\tau e^-$ and derive limits on the dipole moments μ_{ν_τ} and d_{ν_τ} at 2σ and 3σ level (90% and 95% C.L.) via Weisacker-Williams approximation, and at a future high-energy and high-luminosity linear electron positron collider, such as the ILC and CLIC to study the sensibility on the anomalous magnetic and electric dipole moments of the tau neutrino.

For this we calculate the main reaction $e^+e^- \to e^+\gamma^*e^- \to e^+\tau\bar{\nu}_\tau\nu_e$ by integrating the cross section for the subprocess $\gamma^*e^- \to \tau\bar{\nu}_\tau\nu_e$. The acceptance cuts will be imposed as $|\eta^\tau| < 2.5$ for pseudorapidity and $p_T^\tau > 20$ GeV for the transverse momentum cut of the final state τ lepton, respectively. For the second process we calculate the main reaction $e^+e^- \to e^+\gamma^*\gamma^*e^- \to e^+\nu_\tau\bar{\nu}_\tau e^-$. Neutrinos in this process are not detected directly in the central detector. Therefore, we do not apply any cuts for the final state particles. The corresponding Feynman diagrams for the main reactions as well as for the subprocesses that give the most important contribution to the total cross section are shown in Figs. 1–4.

To illustrate our results for both processes we show the dependence of the total cross section as a function of anomalous couplings F_2 and F_3 for three different values of the center-of-mass energies 0.5,1.5, and 3 TeV,

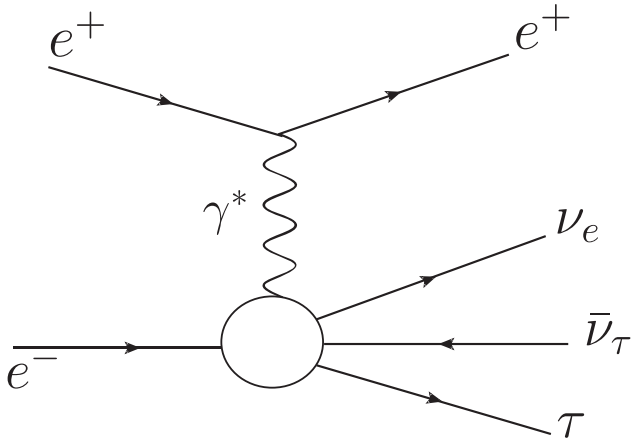

FIG. 1. Schematic diagram for the process $e^+e^- \to e^+\gamma^*e^- \to e^+\tau\bar{\nu}_\tau\nu_e$.

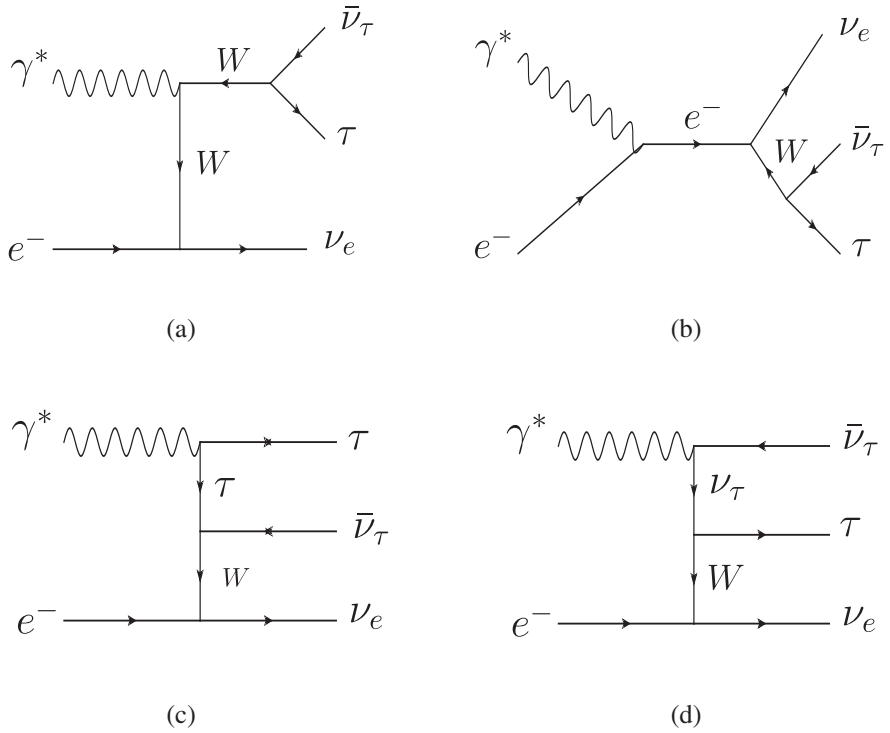

FIG. 2. The Feynman diagrams contributing to the subprocess $\gamma^* e^- \to \tau\bar{\nu}_\tau\nu_e$. The diagrams (a)–(c) correspond to the contribution of the standard model, while diagram (d) corresponds to the anomalous contribution.

respectively. The variation of the cross section as a function of F_2 and F_3 for different values of Q^2 (Weizsacker-Williams photon virtuality) and center-of-mass energy of 0.5,1.5, and 3 TeV is evaluated. We also include a contours plot for the upper bounds of the anomalous couplings μ_{ν_τ} and d_{ν_τ} with 95% C.L. at the $\sqrt{s} = 0.5$, 1.5, 3 TeV with corresponding maximum luminosities for both processes.

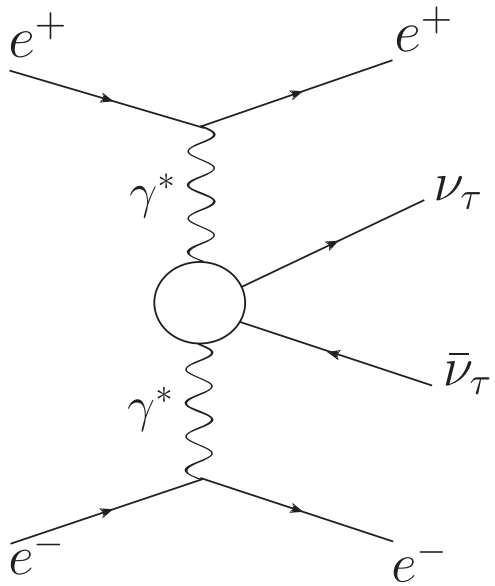

FIG. 3. Schematic diagram for the process $e^+e^- \to e^+\gamma^*\gamma^*e^- \to e^+\nu_\tau\bar{\nu}_\tau e^-$.

The sensitivity limits on the magnetic moment μ_{ν_τ} and the electric dipole moment d_{ν_τ} of the tau neutrino for different values of photon virtuality, center-of-mass energy, and luminosity are also calculated.

This paper is organized as follows. In Sec. II, we study the dipole moments of the tau neutrino through the processes $e^+e^- \to e^+\gamma^*e^- \to e^+\tau\bar{\nu}_\tau\nu_e$ in the γ^*e^- collision mode and $e^+e^- \to e^+\gamma^*\gamma^*e^- \to e^+\nu_\tau\bar{\nu}_\tau e^-$ through the $\gamma^*\gamma^*$ collision mode. Finally, we present our results and conclusions in Sec. III.

II. CROSS SECTION OF $e^+e^- \to e^+\gamma^*e^- \to e^+\tau\bar{\nu}_\tau\nu_e$ AND $e^+e^- \to e^+\gamma^*\gamma^*e^- \to e^+\nu_\tau\bar{\nu}_\tau e^-$

In this section we present numerical results of the cross section for both processes $e^+e^- \to e^+\gamma^*e^- \to e^+\tau\bar{\nu}_\tau\nu_e$ and

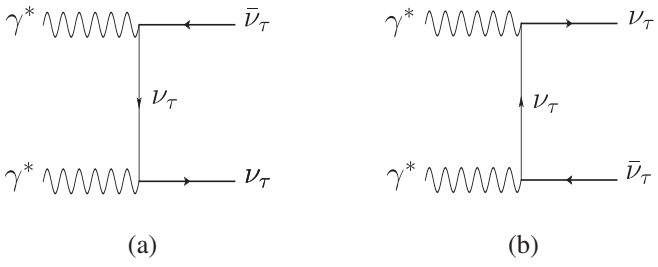

FIG. 4. The Feynman diagrams contributing to the subprocess $\gamma^*\gamma^* \to \nu_\tau\bar{\nu}_\tau$. The diagrams (a) and (b) correspond to the anomalous contribution.

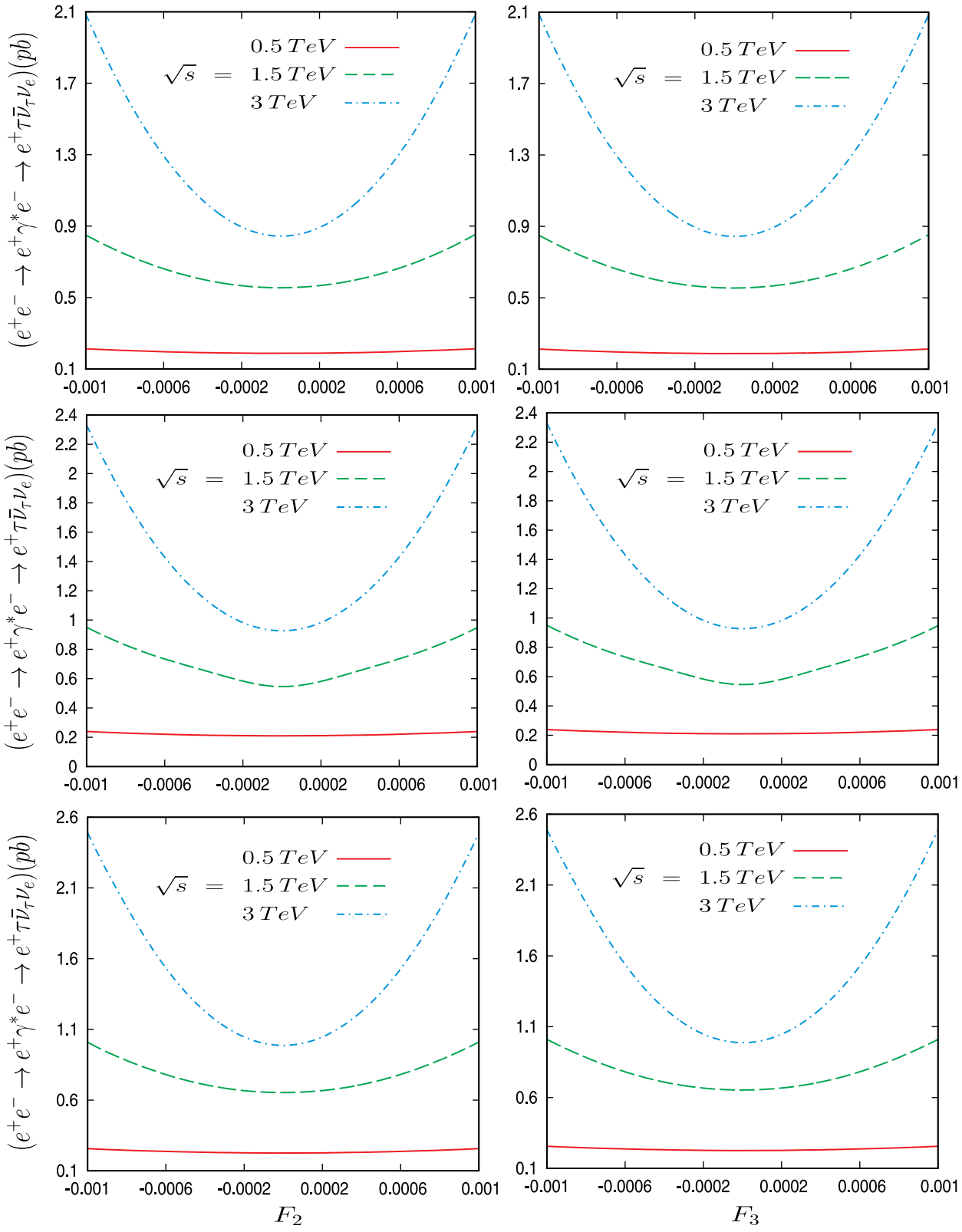

FIG. 5 (color online). The integrated total cross section of the process $e^+e^- \to e^+\gamma^* e^- \to e^+\tau\bar{\nu}_\tau\nu_e$ as a function of the anomalous couplings F_2 and F_3 for three different center-of-mass energies $\sqrt{s} = 0.5$, 1.5, 3 TeV and $Q^2 = 2, 16, 64$ GeV^2, respectively.

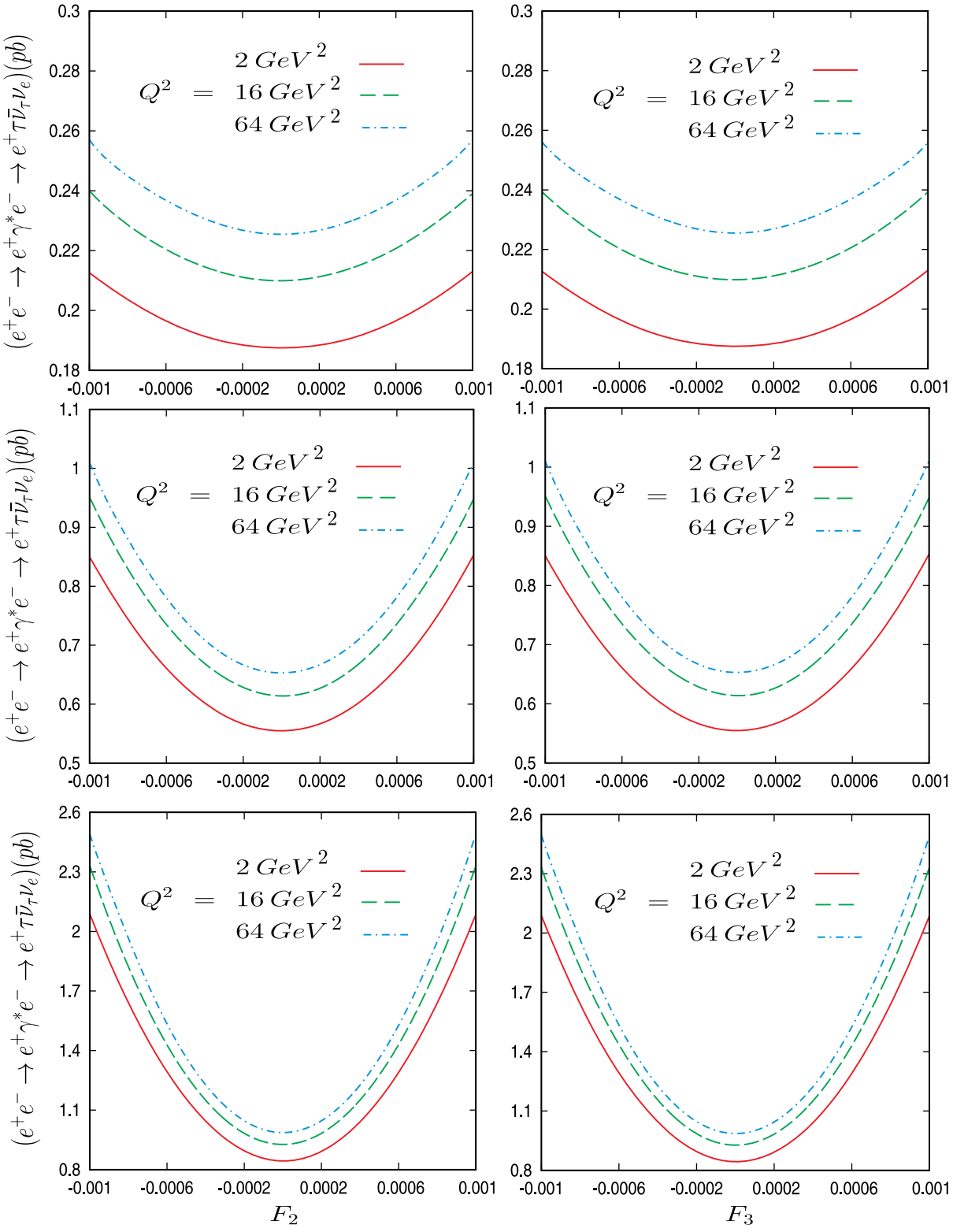

FIG. 6 (color online). The total cross section of the process $e^+e^- \to e^+\gamma^*e^- \to e^+\tau\bar{\nu}_\tau\nu_e$ as a function of the anomalous couplings F_2 and F_3 for three different values of $Q^2 = 2, 16, 64$ GeV^2 and center-of-mass energies $\sqrt{s} = 0.5,\ 1.5,\ 3$ TeV, respectively.

$e^+e^- \to e^+\gamma^*\gamma^*e^- \to e^+\nu_\tau\bar{\nu}_\tau e^-$ as a function of the electromagnetic form factors of the neutrino F_2 and F_3. In addition, to see the sensitivity of the magnetic moment μ_{ν_τ} and the electric dipole moment d_{ν_τ} to new physics, we plot $\mu_{\nu_\tau}(d_{\nu_\tau})$ versus $\mathcal{L}$. We carry out the calculations using the framework of the minimally extended standard model at next generation linear γ^*e^- and $\gamma^*\gamma^*$ collisions: ILC and CLIC.

We use the CompHEP [58] packages for calculations of the matrix elements and cross sections. These packages provide automatic computation of the cross sections and distributions in the SM as well as their extensions at tree level. We consider the high-energy stage of possible future linear γ^*e^- and $\gamma^*\gamma^*$ collisions with $\sqrt{s} = 0.5$, 1.5 and 3 TeV and design luminosity 230, 320, and 590 fb^{-1} according to the data reported by the ILC and CLIC [43,44]. In addition, we consider the acceptance cuts of $|\eta^\tau| < 2.5$ for pseudorapidity and $p_T^\tau > 20$ GeV for a transverse momentum cut of the final state τ lepton, respectively.

A. Magnetic moment and electric dipole moment via $e^+e^- \to e^+\gamma^*e^- \to e^+\tau\bar{\nu}_\tau\nu_e$

The corresponding Feynman diagrams for the main reaction $e^+e^- \to e^+\gamma^*e^- \to e^+\tau\bar{\nu}_\tau\nu_e$, as well as for the subprocess $\gamma^*e^- \to \tau\bar{\nu}_\tau\nu_e$, that give the most important contribution to the total cross section are shown in Figs. 1–2. From Fig. 2, the Feynman diagrams (a)–(c) correspond to the contribution of the standard model, while diagram (d) corresponds to the anomalous contribution, which is to say, for the γ^*e^- collisions there are SM backgrounds at the tree level so the total cross section is proportional to $\sigma_{\rm Tot} = \sigma_{\rm SM} + \sigma_{\rm Int}(F_2, F_3) + \sigma_{\rm Anom}(F_2^2, F_3^2, F_2F_3)$, respectively.

To illustrate our results we show the dependence of the cross section on the anomalous couplings F_2 and F_3 for $e^+e^- \to e^+\gamma^*e^- \to e^+\tau\bar{\nu}_\tau\nu_e$ in Fig. 5 for three different center-of-mass energies $\sqrt{s} = 0.5$, 1.5, 3 TeV and $Q^2 = 2, 16, 64$ GeV^2 [16], respectively. The cross section is sensitive to the value of the center-of-mass energies, as well as to Q^2. The sensitivity to $e^+\tau\bar{\nu}_\tau\nu_e$ increases with the collider energy, as well as with Q^2 reaching a maximum at the end of the range considered: $F_{2,3} = \pm 0.001$. In Fig. 6, we show again the total cross section, but now for different values of $Q^2 = 2, 16, 64$ GeV^2 [16] and center-of-mass energies of $\sqrt{s} = 0.5$, 1.5, 3 TeV. We observed that the variation of the cross section for $e^+\tau\bar{\nu}_\tau\nu_e$ as a function of the anomalous couplings F_2 and F_3 is clear for all cases.

In Figs. 7–8 we present the dependence of the sensitivity limits of the magnetic moment μ_{ν_τ} and the electric dipole moment d_{ν_τ} with respect to the collider luminosity $\mathcal{L}$ for three different values of the Weizsacker-Williams photon virtuality $Q^2 = 2, 16, 64$ GeV^2 and center-of-mass energies of $\sqrt{s} = 0.5$, 1.5, 3 TeV. In these figures, we observe one variation of $\mu_{\nu_\tau}(d_{\nu_\tau})$ in all the intervals of $\mathcal{L}$, and it is almost independent of the value of Q^2.

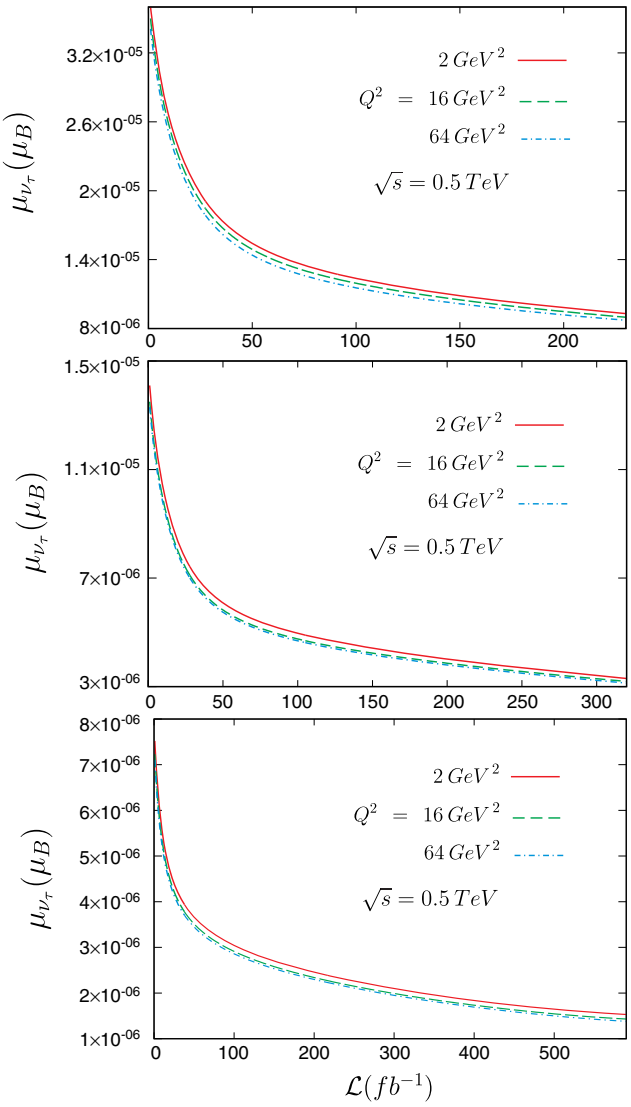

FIG. 7 (color online). Dependence of the sensitivity limits at 95% C.L. for the anomalous magnetic moment for three different values of $Q^2 = 2, 16, 64$ GeV^2 and center-of-mass energies $\sqrt{s} = 0.5, 1.5, 3$ TeV in the subprocess $\gamma^*e^- \to \tau\bar{\nu}_\tau\nu_e$.

As an indicator of the order of magnitude, in Tables II–III we present the bounds obtained on the μ_{ν_τ} magnetic moment and d_{ν_τ} electric dipole moment for $Q^2 = 2, 64$ GeV^2, $\sqrt{s} = 0.5$, 1.5, 3 TeV, and $\mathcal{L} = 230$, 320, 590 fb^{-1} at 2σ and 3σ C.L., respectively. We observed that the results obtained in Tables II–III are competitive with those reported in the literature [20–22]. For the electric dipole moment our limits compare favorably with those reported by Akama *et al.* [34] [$|d_{\nu_\tau}| < O(2 \times 10^{-17} ecm)$] and R. Escribano and Massó [12] ($|d_{\nu_\tau}| \leq 5.2 \times 10^{-17} ecm$, 95% C.L.).

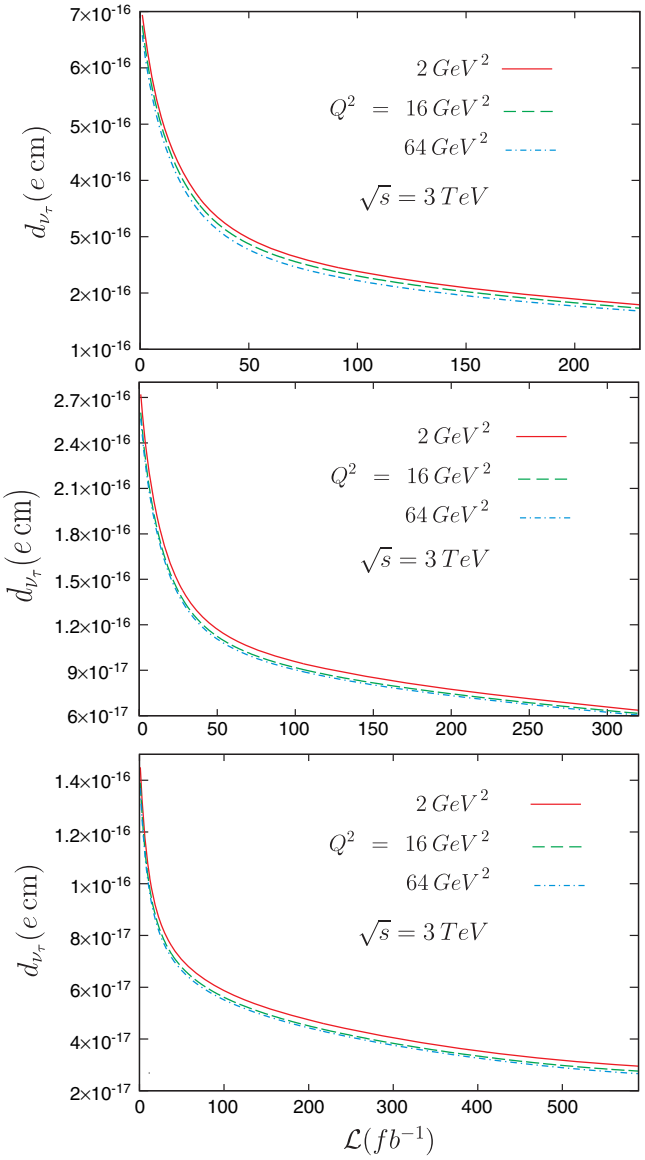

FIG. 8 (color online). The same as Fig. 7 but for the electric dipole moment.

In Fig. 9 we used three center-of-mass energies $\sqrt{s} = 0.5$, 1.5, 3 TeV planned for the ILC and CLIC accelerators in order to get contour limits in the plane $\mu_{\nu_\tau} - d_{\nu_\tau}$ for $e^+e^- \to e^+\gamma^*e^- \to e^+\tau\bar{\nu}_\tau\nu_e$ and the planned luminosities of $\mathcal{L} = 230$, 320, 590 fb^{-1} and Weizsacker-Williams photon virtuality $Q^2 = 2$ GeV^2. For the γ^*e^- collision, we perform χ^2 analysis at 95% C.L. since the number of SM events is greater than 10.

TABLE II. Bounds on the μ_{ν_τ} magnetic moment and d_{ν_τ} electric dipole moment for the process $e^+e^- \to e^+\gamma^*e^- \to e^+\tau\bar{\nu}_\tau\nu_e$ for $Q^2 = 2$ GeV^2, $\sqrt{s} = 0.5$, 1.5, 3 TeV, and $\mathcal{L} = 230$, 320, 590 fb^{-1} at 2σ and 3σ C.L.

$\sqrt{s} = 0.5$, 1.5, 3 TeV, $\mathcal{L} = 230$, 320, 590 fb^{-1}		
C.L.	$\lvert\mu_{\nu_\tau}(\mu_B)\rvert$	$\lvert d_{\nu_\tau}(ecm)\rvert$
2σ	$(8.73, 3.35, 1.60) \times 10^{-6}$	$(16.8, 6.46, 3.08) \times 10^{-17}$
3σ	$(9.30, 3.30, 1.53) \times 10^{-6}$	$(17.9, 6.36, 2.95) \times 10^{-17}$

TABLE III. Bounds on the μ_{ν_τ} magnetic moment and d_{ν_τ} electric dipole moment for the process $e^+e^- \to e^+\gamma^*e^- \to e^+\tau\bar{\nu}_\tau\nu_e$ for $Q^2 = 64$ GeV^2, $\sqrt{s} = 0.5$, 1.5, 3 TeV, and $\mathcal{L} = 230$, 320, 590 fb^{-1} at 2σ and 3σ C.L.

$\sqrt{s} = 0.5$, 1.5, 3 TeV, $\mathcal{L} = 230$, 320, 590 fb^{-1}		
C.L.	$\lvert\mu_{\nu_\tau}(\mu_B)\rvert$	$\lvert d_{\nu_\tau}(ecm)\rvert$
2σ	$(8.22, 2.88, 1.32) \times 10^{-6}$	$(15.8, 5.56, 2.54) \times 10^{-17}$
3σ	$(8.97, 3.14, 1.44) \times 10^{-6}$	$(17.3, 6.06, 2.78) \times 10^{-17}$

B. Magnetic moment and electric dipole moment via $e^+e^- \to e^+\gamma^*\gamma^*e^- \to e^+\nu_\tau\bar{\nu}_\tau e^-$

In this subsection we study the dipole moments of the tau neutrino via the process $e^+e^- \to e^+\gamma^*\gamma^*e^- \to e^+\nu_\tau\bar{\nu}_\tau e^-$ for energies expected at the ILC and CLIC [43,44]. The corresponding Feynman diagrams for the subprocess $\gamma^*\gamma^* \to \nu_\tau\bar{\nu}_\tau$ that give the most important contribution to the total cross section are shown in Figs. 3–4. In this case, the total cross section of the subprocess depends only on the diagrams (a) and (b) with anomalous couplings, and there is no contribution at tree level of the standard model, which is to say $\sigma_{\mathrm{Tot}} = \sigma(F_2^4, F_3^4, F_2^3F_3, F_2^2F_3^2, F_2F_3^3)$.

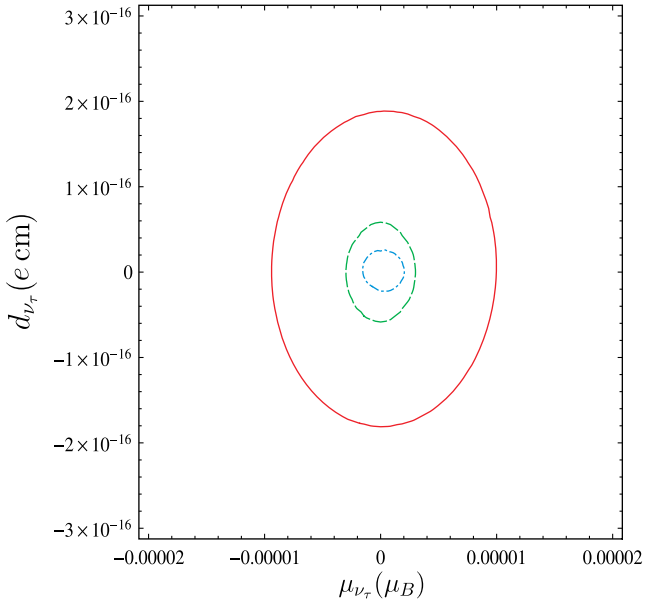

FIG. 9 (color online). Limits contours at the 95% C.L. in the $\mu_{\nu_\tau} - d_{\nu_\tau}$ plane for $e^+e^- \to e^+\gamma^*e^- \to e^+\tau\bar{\nu}_\tau\nu_e$. Starting from the top, the curves are for $\sqrt{s} = 0.5$ TeV and $\mathcal{L} = 230$ fb^{-1}; $\sqrt{s} = 1.5$ TeV and $\mathcal{L} = 320$ fb^{-1}; $\sqrt{s} = 3$ TeV and $\mathcal{L} = 590$ fb^{-1}, respectively. We have used $Q^2 = 2$ GeV^2.

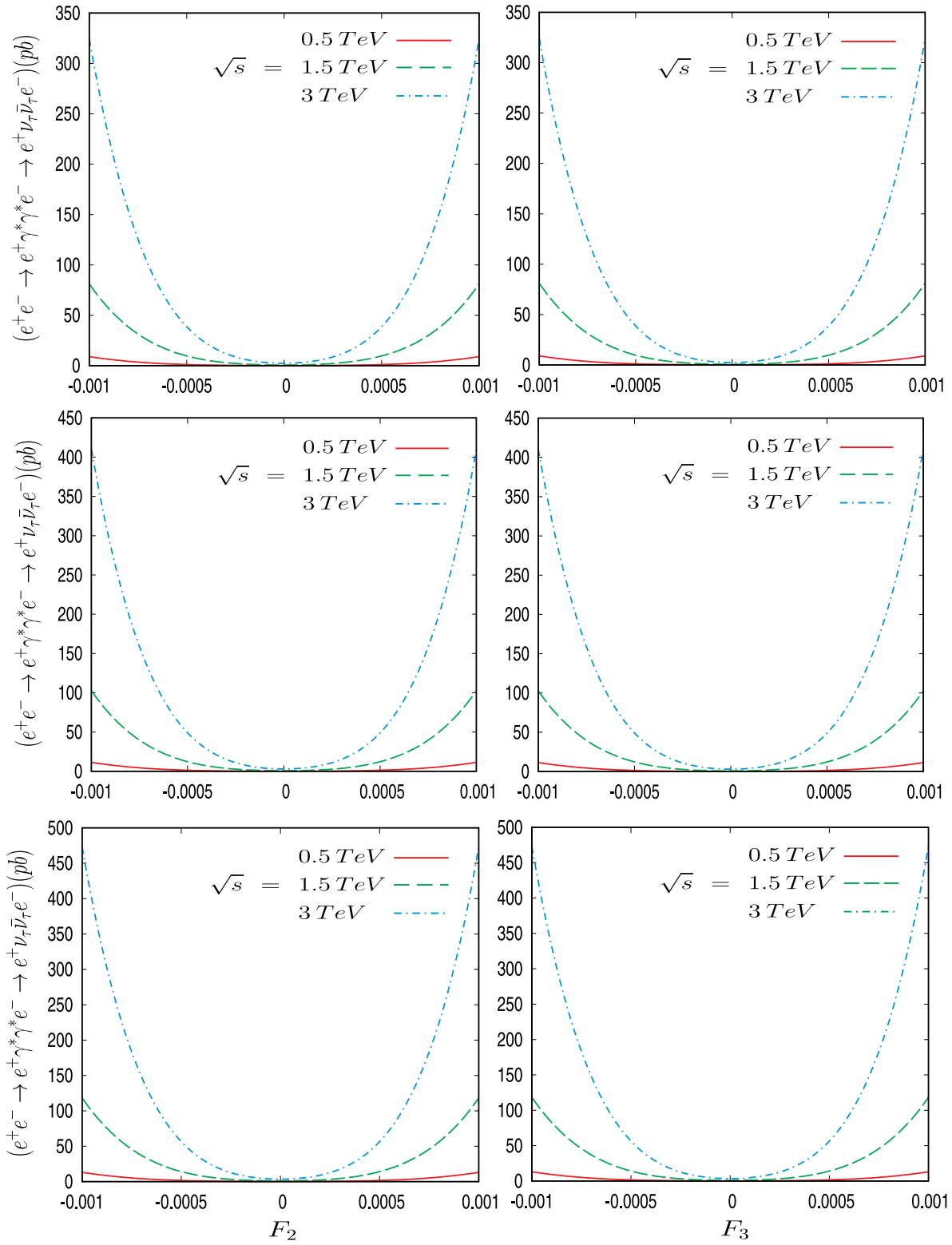

FIG. 10 (color online). The total cross section of the process $e^+e^- \to e^+\gamma^*\gamma^*e^- \to e^+\nu_\tau\bar{\nu}_\tau e^-$ as a function of the anomalous couplings F_2 and F_3 for three different center-of-mass energies $\sqrt{s} = 0.5$, 1.5, 3 TeV and $Q^2 = 2, 16, 64$ GeV^2, respectively.

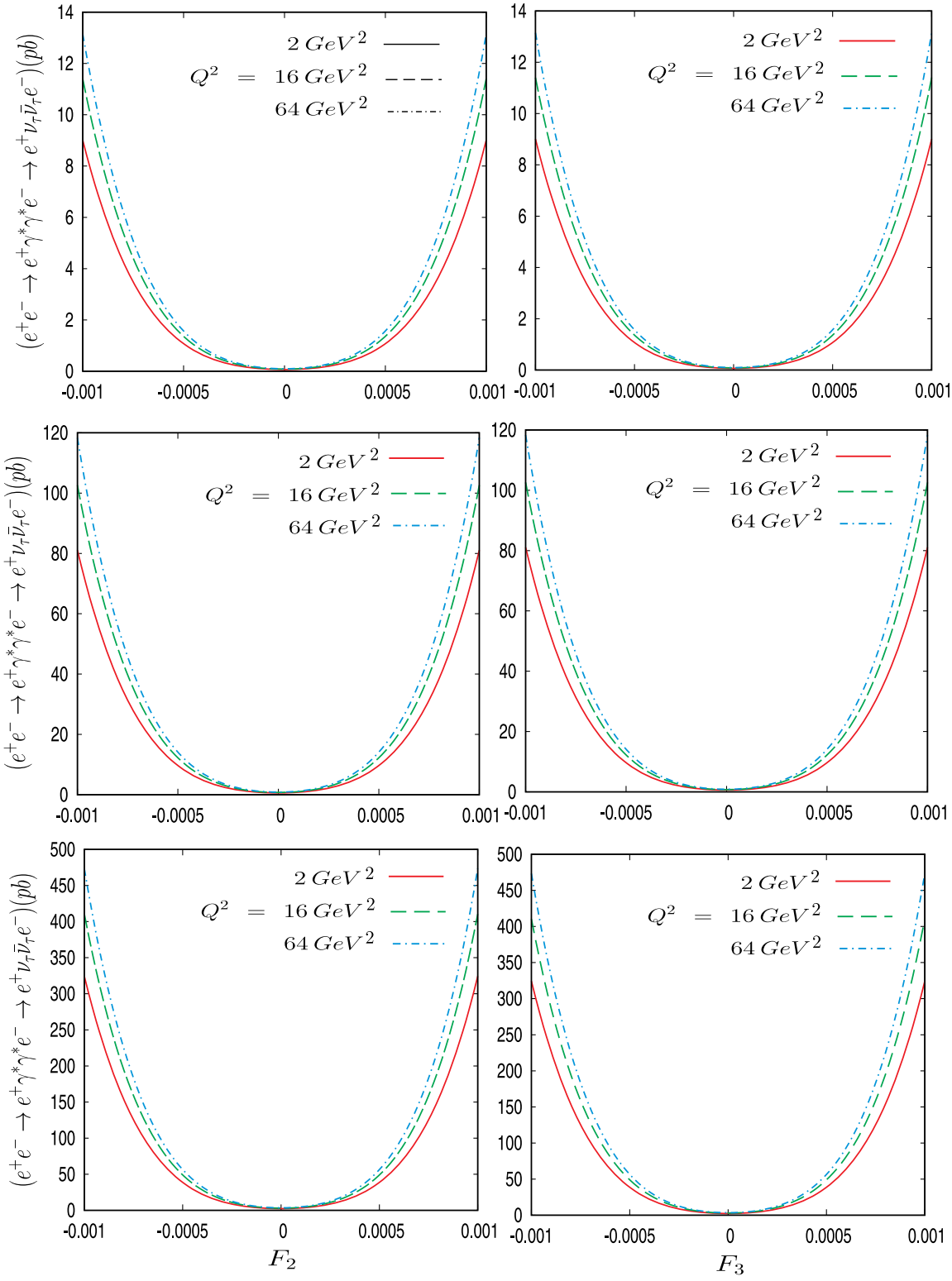

FIG. 11 (color online). The integrated total cross section of the process $e^+e^- \to e^+\gamma^*\gamma^*e^- \to e^+\nu_\iota\bar{\nu}_\tau e^-$ as a function of the anomalous couplings F_2 and F_3 for three different values of $Q^2 = 2, 16, 64$ GeV^2 and center-of-mass energies $\sqrt{s} = 0.5$, 1.5, 3 TeV, respectively.

For the study of the subprocess $\gamma^*\gamma^* \to \nu_\tau\bar{\nu}_\tau$ in Fig. 10, we show the total cross section as a function of the electromagnetic form factors of the neutrino F_2 and F_3 for three different center-of-mass energies $\sqrt{s} = 0.5$, 1.5, 3 TeV and $Q^2 = 2, 16, 64$ GeV^2 [16], respectively. We can see from this figure that the total cross section changes strongly with the variation of the $\sqrt{s}$ and Q^2 values.

As in Sec. II A, we show the F_2 and F_3 dependence of the total cross section for $e^+e^- \to e^+\gamma^*\gamma^*e^- \to e^+\nu_\tau\bar{\nu}_\tau e^-$ in Fig. 11. From this figure we observed a significant dependence of the cross section with respect to F_2 and F_3, and different values of center-of-mass energy $\sqrt{s}$ and Q^2. In Figs. 12–13 we present the dependence of the sensitivity limits of the magnetic moment μ_{ν_τ} and the electric dipole moment d_{ν_τ} with respect to the collider luminosity $\mathcal{L}$ for three different values of $Q^2 = 2, 16, 64$ GeV^2 [16] and center-of-mass energies of $\sqrt{s} = 0.5$, 1.5, 3 TeV.

In Tables IV–V we present the bounds obtained on the μ_{ν_τ} magnetic moment and d_{ν_τ} electric dipole moment for $\sqrt{s} = 0.5$, 1.5, 3 TeV, $Q^2 = 2, 64$ GeV^2, and $\mathcal{L} = 230, 320, 590$ fb^{-1} at 2σ and 3σ. We observed that the results obtained in Tables IV–V improve the bounds reported in the literature [20–22].

In the case of the electric dipole moment the 90, 95% C.L. sensitivity limits at 0.5, 1.5, and 3 TeV center-of-mass energies and integrated luminosities of 230, 320, and 590 fb^{-1}, respectively, can provide proof of these bounds of order 10^{-18}, which is to say, they are improved by one order of magnitude more than those

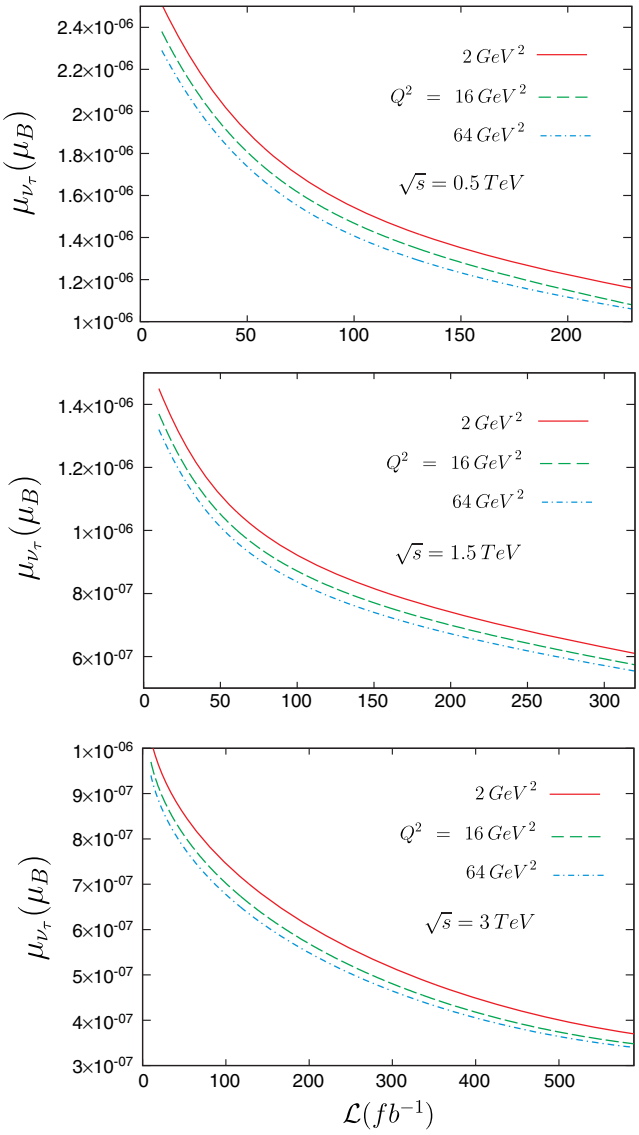

FIG. 12 (color online). Dependence of the sensitivity limits at 95% C.L. for the anomalous magnetic moment for three different values of $Q^2 = 2, 16, 64$ GeV^2 and center-of-mass energies $\sqrt{s} = 0.5$, 1.5, 3 TeV in the subprocess $\gamma^*\gamma^* \to \nu_\tau\bar{\nu}_\tau$.

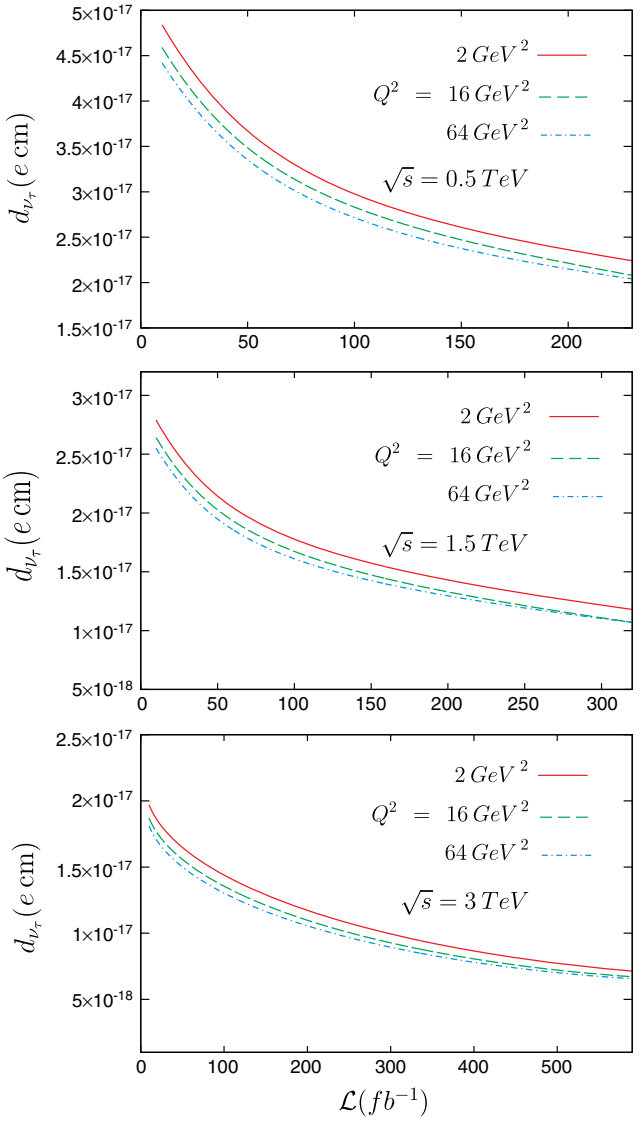

FIG. 13 (color online). The same as Fig. 12 but for the electric dipole moment.

TABLE IV. Bounds on the μ_{ν_τ} magnetic moment and d_{ν_τ} electric dipole moment for the process $e^+e^- \to e^+\gamma^*\gamma^*e^- \to e^+\nu_\tau\bar{\nu}_\tau e^-$ for $Q^2 = 2$ GeV^2, $\sqrt{s} = 0.5$, 1.5, 3 TeV, and $\mathcal{L} = 230, 320, 590$ fb^{-1} at 2σ and 3σ C.L.

$\sqrt{s} = 0.5,\ 1.5,\ 3$ TeV, $\mathcal{L} = 230,\ 320,\ 590$ fb^{-1}		
C.L.	$\lvert\mu_{\nu_\tau}(\mu_B)\rvert$	$\lvert d_{\nu_\tau}(ecm)\rvert$
2σ	$(10.90, 5.70, 3.50) \times 10^{-7}$	$(2.10, 1.09) \times 10^{-17}, 6.75 \times 10^{-18}$
3σ	$(11.60, 6.10, 3.70) \times 10^{-7}$	$(2.24, 1.18) \times 10^{-17}, 7.14 \times 10^{-18}$

TABLE V. Bounds on the μ_{ν_τ} magnetic moment and d_{ν_τ} electric dipole moment for the process $e^+e^- \to e^+\gamma^*\gamma^*e^- \to e^+\nu_\tau\bar{\nu}_\tau e^-$ for $Q^2 = 64$ GeV^2, $\sqrt{s} = 0.5$, 1.5, 3 TeV, and $\mathcal{L} = 230, 320, 590$ fb^{-1} at 2σ and 3σ C.L.

$\sqrt{s} = 0.5,\ 1.5,\ 3$ TeV, $\mathcal{L} = 230,\ 320,\ 590$ fb^{-1}		
C.L.	$\lvert\mu_{\nu_\tau}(\mu_B)\rvert$	$\lvert d_{\nu_\tau}(ecm)\rvert$
2σ	$(9.90, 5.20, 3.10) \times 10^{-7}$	$(1.91, 1.00) \times 10^{-17}, 5.98 \times 10^{-18}$
3σ	$(10.60, 5.54, 3.40) \times 10^{-7}$	$(2.04, 1.07) \times 10^{-17}, 6.56 \times 10^{-18}$

reported in the literature: $|d_{\nu_\tau}| < O(2 \times 10^{-17} ecm)$ [34] and $|d_{\nu_\tau}| \leq 5.2 \times 10^{-17} ecm$, 95% C.L. [12].

Finally, in Fig. 14 we summarize the respective limit contours for the dipole moments in the $\mu_{\nu_\tau} - d_{\nu_\tau}$ plane for $e^+e^- \to e^+\gamma^*\gamma^*e^- \to e^+\nu_\tau\bar{\nu}_\tau e^-$. Starting from the top, the curves are for $\sqrt{s} = 0.5$ TeV and $\mathcal{L} = 230$ fb^{-1}; $\sqrt{s} =$ 1.5 TeV and $\mathcal{L} = 320$ fb^{-1}; $\sqrt{s} = 3$ TeV and $\mathcal{L} = 590$ fb^{-1}, respectively. We have used $Q^2 = 2$ GeV^2. In this case for the $\gamma^*\gamma^*$ collision, we perform Poisson analysis at 95% C.L. since the number of SM events is smaller than 10.

III. CONCLUSIONS

Even though γe^- and $\gamma\gamma$ processes require new equipment, $\gamma^* e^-$ and $\gamma^*\gamma^*$ are realized spontaneously at linear colliders without any equipment. These processes will allow the next generation linear collider to operate in three different modes, e^+e^-, $\gamma^* e^-$, and $\gamma^*\gamma^*$, opening up the opportunity for a wider search for new physics. Therefore, the $\gamma^* e^-$ and $\gamma^*\gamma^*$ linear collisions represent an excellent opportunity to study the sensibility on the anomalous magnetic moment and electric dipole moment of the tau neutrino.

We have done an analysis of the total cross section of the processes $e^+e^- \to e^+\gamma^*e^- \to e^+\tau\bar{\nu}_\tau\nu_e$ and $e^+e^- \to e^+\gamma^*\gamma^*e^- \to e^+\nu_\tau\bar{\nu}_\tau e^-$ as a function of the anomalous coupling F_2 and F_3. The analysis is shown in Figs. 5–6 and 10–11 for different center-of-mass energies and several values of the Weizsacker-Williams photon virtuality. In all cases, the cross section shows a strong dependence on the anomalous couplings F_2 and F_3.

The correlation between the luminosity $\mathcal{L}$ of the collider and the anomalous magnetic moment μ_{ν_τ} and the electric dipole moment d_{ν_τ} is presented in Figs. 7–8. In both cases, we see that there is a strong correlation between $\mathcal{L}$ and the dipole moments; the same is also observed in Figs. 12–13 as well as in Tables II–V.

We also include contour plots for the dipole moments at the 95% C.L. in the $\mu_{\nu_\tau} - d_{\nu_\tau}$ plane for $Q^2 = 2$ GeV^2 and $\sqrt{s} = 0.5$, 1.5, 3 TeV in Figs. 9 and 14. The contours are obtained from Tables II–V.

It is worth mentioning that our bounds obtained in Tables II–V on the anomalous magnetic moment for the processes $e^+e^- \to e^+\gamma^*e^- \to e^+\tau\bar{\nu}_\tau\nu_e$ and $e^+e^- \to$

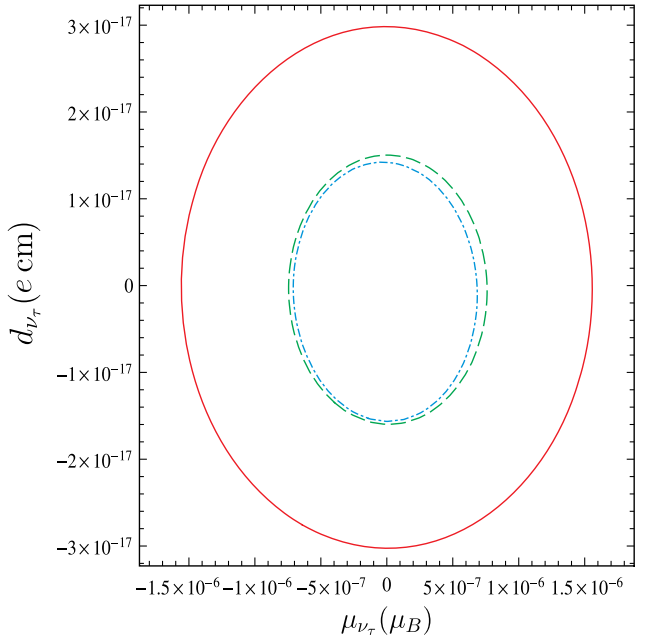

FIG. 14 (color online). Limits contours at the 95% C.L. in the $\mu_{\nu_\tau} - d_{\nu_\tau}$ plane for $e^+e^- \to e^+\gamma^*\gamma^*e^- \to e^+\nu_\tau\bar{\nu}_\tau e^-$. Starting from the top, the curves are for $\sqrt{s} = 0.5$ TeV and $\mathcal{L} = 230$ fb^{-1}; $\sqrt{s} = 1.5$ TeV and $\mathcal{L} = 320$ fb^{-1}; $\sqrt{s} = 3$ TeV and $\mathcal{L} = 590$ fb^{-1}, respectively. We have used $Q^2 = 2$ GeV^2.

$e^+\gamma^*\gamma^*e^- \to e^+\nu_\tau\bar{\nu}_\tau e^-$ for $Q^2 = 2,64\ \mathrm{GeV}^2$, $\sqrt{s} = 0.5, 1.5, 3$ TeV, and $\mathcal{L} = 230, 320, 590\ \mathrm{fb}^{-1}$ at 2σ and 3σ C.L. compare favorably with the bounds obtained in Table I by the DONUT [20], WA66 [21], and L3 collaborations [22], as well as those reported by Akama *et al.* [34] [$\mu_{\nu_\tau} < O(1.1 \times 10^{-6}\mu_B)$] and R. Escribano and Massó [12] ($\mu_{\nu_\tau} \leq 2.7 \times 10^{-6}\mu_B$ 95% C.L.); whereas, in the case of the electric dipole moment our results obtained in Tables II–V are improved by one order of magnitude more than those reported in the literature [$|d_{\nu_\tau}| < O(2 \times 10^{-17} ecm)$ [34] and $|d_{\nu_\tau}| \leq 5.2 \times 10^{-17} ecm$, 95% C.L. [12]].

In conclusion, we have found that the processes $e^+e^- \to e^+\gamma^*e^- \to e^+\tau\bar{\nu}_\tau\nu_e$ and $e^+e^- \to e^+\gamma^*\gamma^*e^- \to e^+\nu_\tau\bar{\nu}_\tau e^-$ in the γ^*e^- and $\gamma^*\gamma^*$ collision modes at the high energies and luminosities expected at the ILC and CLIC colliders can be used to probe for bounds on the magnetic moment μ_{ν_τ} and electric dipole moment d_{ν_τ} of the tau neutrino. In particular, we can appreciate that for integrated luminosities of 590 fb^{-1} and center-of-mass energies of 3 TeV, we derive 95% C.L. limits on the dipole moments: $\mu_{\nu_\tau} \leq 1.44 \times 10^{-6}\mu_B$ and $d_{\nu_\tau} \leq 2.78 \times 10^{-17} ecm$ for the process $e^+e^- \to e^+\gamma^*e^- \to e^+\tau\bar{\nu}_\tau\nu_e$ and of $\mu_{\nu_\tau} \leq 3.4 \times 10^{-7}\mu_B$ and $d_{\nu_\tau} \leq 6.56 \times 10^{-18} ecm$ for $e^+e^- \to e^+\gamma^*\gamma^*e^- \to e^+\nu_\tau\bar{\nu}_\tau e^-$, better than those reported in the literature.

ACKNOWLEDGMENTS

A. G. R. acknowledges support from Consejo Nacional de Ciencia y Tecnología (CONACyT), Sistema Nacional de Investigadores (SNI), Programa de Mejoramiento al Profesorado (PROMEP) and Programa Integral de Fortalecimiento Institucional (PIFI) (México).

[1] S. L. Glashow, Nucl. Phys. **22**, 579 (1961).
[2] S. Weinberg, Phys. Rev. Lett. **19**, 1264 (1967).
[3] A. Salam, in *Elementary Particle Theory*, edited by N. Svartholm (Almquist and Wiskell, Stockholm, 1968), p. 367.
[4] K. Fujikawa and R. Shrock, Phys. Rev. Lett. **45**, 963 (1980).
[5] Robert E. Shrock, Nucl. Phys. **B206**, 359 (1982).
[6] M. Fukugita and T. Yanagida, *Physics of Neutrinos and Applications to Astrophysics* (Springer, Berlin, 2003).
[7] A. Cisneros, Astrophys. Space Sci. **10**, 87 (1971).
[8] G. G. Raffelt, Phys. Rep. **320**, 319 (1999).
[9] A. G. Beda *et al.* (GEMMA Collaboration), Adv. High Energy Phys. **2012**, 1 (2012).
[10] L. B. Auerbach *et al.* (LSND Collaboration), Phys. Rev. D **63**, 112001 (2001).
[11] F. del Aguila and M. Sher, Phys. Lett. B **252**, 116 (1990).
[12] R. Escribano and E. Massó, Phys. Lett. B **395**, 369 (1997).
[13] P. Vogel and J. Engel, Phys. Rev. D **39**, 3378 (1989).
[14] J. Bernabeu, L. Cabral-Rosetti, J. Papavassiliou, and J. Vidal, Phys. Rev. D **62**, 113012 (2000).
[15] J. Bernabeu, J. Papavassiliou, and J. Vidal, Phys. Rev. Lett. **89**, 101802 (2002); **89**, 229902 (2002).
[16] M. S. Dvornikov and A. I. Studenikin, J. Exp. Theor. Phys. **99**, 254 (2004).
[17] C. Giunti and A. Studenikin, Phys. At. Nucl. **72**, 2089 (2009).
[18] C. Broggini, C. Giunti, and A. Studenikin, Adv. High Energy Phys. **2012**, 1 (2012); arXiv:1207.3980.
[19] C. Arpesella *et al.* (Borexino Collaboration), Phys. Rev. Lett. **101**, 091302 (2008).
[20] R. Schwinhorst *et al.* (DONUT Collaboration), Phys. Lett. B **513**, 23 (2001).
[21] A. M. Cooper-Sarkar, S. Sarkar, J. Guy, W. Venus, P. O. Hulth, and K. Hultqvist (WA66 Collaboration), Phys. Lett. B **280**, 153 (1992).
[22] M. Acciarri *et al.* (L3 Collaboration), Phys. Lett. B **412**, 201 (1997).
[23] A. Gutiérrez-Rodríguez, Int. J. Theor. Phys. **54**, 236 (2015).
[24] A. Gutiérrez-Rodríguez, Adv. High Energy Phys. **2014**, 491252 (2014).
[25] K. A. Olive *et al.* (Particle Data Group), Chin. Phys. **C38**, 090001 (2014).
[26] A. Gutiérrez-Rodríguez, Pramana J. Phys. **79**, 903 (2012).
[27] A. Gutiérrez-Rodríguez, Eur. Phys. J. C **71**, 1819 (2011).
[28] C. Aydin, M. Bayar, and N. Kilic, Chin. Phys. **C32**, 608 (2008).
[29] A. Gutiérrez-Rodríguez, M. A. Hernández-Ruíz, B. Jayme-Valdés, and M. A. Pérez, Phys. Rev. D **74**, 053002 (2006).
[30] M. A. Pérez, G. Tavares-Velasco, and J. J. Toscano, Int. J. Mod. Phys. A **19**, 159 (2004).
[31] A. Gutiérrez-Rodríguez, M. A. Hernández-Ruíz, and A. Del Rio–De Santiago, Phys. Rev. D **69**, 073008 (2004).
[32] A. Gutiérrez-Rodríguez and M. A. Hernández-Ruíz, Acta Phys. Slov. **53**, 293 (2003).
[33] F. Larios, M. A. Pérez, and G. Tavares-Velasco, Phys. Lett. B **531**, 231 (2002).
[34] K. Akama, T. Hattori, and K. Katsuura, Phys. Rev. Lett. **88**, 201601 (2002).
[35] A. Aydemir and R. Sever, Mod. Phys. Lett. A **16**, 457 (2001).
[36] A. Gutiérrez-Rodríguez, M. A. Hernández-Ruíz, A. Rosado, and M. Maya, Rev. Mex. Fis. **45**, 249 (1999).
[37] J. M. Hernández, M. A. Pérez, G. Tavares-Velasco, and J. J. Toscano, Phys. Rev. D **60**, 013004 (1999).
[38] M. Maya, M. A. Pérez, G. Tavares-Velasco, and B. Vega, Phys. Lett. B **434**, 354 (1998).
[39] A. Gutiérrez-Rodríguez, M. A. Hernández, M. Maya, and A. Rosado, Phys. Rev. D **58**, 117302 (1998).
[40] P. Abreu *et al.* (DELPHI Collaboration), Z. Phys. C **74**, 577 (1997).

[41] T. M. Gould and I. Z. Rothstein, Phys. Lett. B **333**, 545 (1994).
[42] H. Grotch and R. Robinet, Z. Phys. C **39**, 553 (1988).
[43] T. Abe *et al.* (Am. LC Group), arXiv:hep-ex/0106057; G. Aarons *et al.* (ILC Collaboration), arXiv:0709.1893; J. Brau *et al.* (ILC Collaboration), arXiv:0712.1950; H. Baer, T. Barklow, K. Fujii *et al.*, arXiv:1306.6352.
[44] E. Accomando *et al.* (CLIC Phys. Working Group Collaboration), Report No. CERN-2004-005; D. Dannheim, P. Lebrun, L. Linssen *et al.*, arXiv:1208.1402; H. Abramowicz *et al.* (CLIC Detector and Physics Study Collaboration), arXiv:1307.5288.
[45] V. M. Budnev, I. F. Ginzburg, G. V. Meledin, and V. G. Serbo, Phys. Rep. **15**, 181 (1975).
[46] G. Baur *et al.*, Phys. Rep. **364**, 359 (2002).
[47] K. Piotrzkowski, Phys. Rev. D **63**, 071502 (2001).
[48] A. Abulencia *et al.* (CDF Collaboration), Phys. Rev. Lett. **98**, 112001 (2007).
[49] T. Aaltonen *et al.* (CDF Collaboration), Phys. Rev. Lett. **102**, 222002 (2009).
[50] T. Aaltonen *et al.* (CDF Collaboration), Phys. Rev. Lett. **102**, 242001 (2009).
[51] S. Chatrchyan *et al.* (CMS Collaboration), J. High Energy Phys. 01 (2012) 052.
[52] S. Chatrchyan *et al.* (CMS Collaboration), J. High Energy Phys. 11 (2012) 080.
[53] V. M. Abazov *et al.* (D0 Collaboration), Phys. Rev. D **88**, 012005 (2013).
[54] S. Chatrchyan *et al.* (CMS Collaboration), J. High Energy Phys. 07 (2013) 116.
[55] J. Abdallah *et al.* (DELPHI Collaboration), Eur. Phys. J. C **35**, 159 (2004).
[56] I. Sahin, Phys. Rev. D **85**, 033002 (2012).
[57] I. Sahin and M. Koksal, J. High Energy Phys. 03 (2011) 100.
[58] A. Pukhov *et al.*, Report No. INP MSU 98-41/542.